WELDING RESEARCH

SUPPLEMENT TO THE WELDING JOURNAL, APRIL 1981
Sponsored by the American Welding Society and the Welding Research Council

RESEARCH/DEVELOPMENT/RESEARCH/DEVELOPMENT/RESEARCH/DEVELOPMENT/RESEARCH/DEVELOPMENT/RESEARCH/DEVELOPMENT/RESEARCH/DEVELOPMENT

Ferrite Morphology and Variations in Ferrite Content in Austenitic Stainless Steel Welds

Variations in ferrite content within the weld are related to weld metal composition, ferrite morphology, and the dissolution of ferrite resulting from thermal cycles during subsequent weld passes

BY S. A. DAVID

ABSTRACT. Four distinct ferrite morphologies have been identified in Type 308 stainless steel multipass welds: vermicular, lacy, acicular, and globular. The first three ferrite types are related to transformations following solidification and the fourth is related to the shape instability of the residual ferrite.

An earlier study showed that most of the ferrite observed in austenitic stainless steel welds containing a duplex structure may be identified as residual primary ferrite resulting from incomplete $\delta \rightarrow \gamma$ transformation during solidification and/or residual ferrite after Widmanstätten austenite precipitation in primary ferrite. These modes of ferrite formation can be used to explain observed ferrite morphologies in austenitic stainless steel welds.

Variations in ferrite content within the weld were also related to weld metal composition, ferrite morphology, and dissolution of ferrite resulting from thermal cycles during subsequent weld passes. An investigation of the Type 308 stainless steel filler metal solidified over cooling rates ranging from 7 to 1600°C/s (44.6 to 2912°F/s) showed that the cooling rate of the weld metal within the freezing range of the alloy affects the amount of ferrite in the microstructure very little. However, the scale of the solidification substructure associated with various solidification rates may influence the ferrite dissolution kinetics.

Introduction

Though several studies[1-3] show that a certain amount of ferrite should be present in austenitic stainless steel welds to prevent hot cracking, the mechanism is not well understood. Although several researchers have proposed 3 to 5 ferrite number (FN) as the required amount to prevent hot cracking, the true amount of ferrite present or required during the critical stage of weld metal solidification is unknown.

Ferrite has also been found[4-8] to influence the strength and corrosion behavior of austenitic stainless steel welds in various ways. For a given composition ferrite may be present in various amounts and in different morphologies within the weld depending on the welding processes and parameters. Recently, Devine[9] found that the amount and morphology of ferrite influence the sensitization behavior of duplex stainless steel. In particular, for a given carbon content, a critical amount and distribution of δ-γ boundary area exist above which the alloy is immune to sensitization. It can therefore be seen that ferrite morphology plays an important role in weld behavior.

Ferrite morphology and variations in ferrite content within a weld have received very little attention.[10,11] Recently, Suutala, Takalo, and Moisio[12,13] referred to three types of weld metal microstructures based on the composition and solidification mode. Though their classification may adequately describe the general microstructures, it does not refer to distinct ferrite morphologies and other forms of ferrite often observed in weld metal microstructures. Lai and Townsend[14] have noted that the vermicular and needle-like ferrite morphologies described by Takalo and Moisio[15] are one and the same. For austenitic stainless steel welds containing duplex structure, the

Paper to be presented at the 62nd AWS Annual Meeting in Cleveland, Ohio, during April 5-10, 1981.

S. A. DAVID is a Research Staff Member, Oak Ridge National Laboratory, Oak Ridge, Tennessee.

term "typical microstructure" is often misleading.

Generally, the weld metal has no single representative microstructure but rather is a combination of microstructures with various ferrite forms influenced by such factors as local variations in cooling rate, composition, etc. Hence, detailed observation and classification of ferrite in welds based on its distinct shape and form are needed. In addition to the influence of composition on the ferrite morphology, effects of cooling rate and the thermal excursions during a multipass weld commonly influence ferrite content in austenitic stainless steel welds. The variation in ferrite content has often been attributed to the inadequacies of the present ferrite measuring devices.

In addition to the problems associated with the accuracy of ferrite measurement techniques, a number of other factors contribute to the observed variations in measured ferrite content within the weld metal: composition, ferrite morphology, dissolution and/or transformation of ferrite due to thermal cycles, and cooling rate. The composition of the weld metal expressed as a ratio of chromium to nickel equivalents (Cr_{eq}/Ni_{eq})* is one of the major factors determining the ferrite content of the weld.

The Schaeffler[16] constitution diagram originally provided a method for calculating as-welded ferrite content. This constitution diagram was further modified by DeLong and others[17,18] to take into account the austenitizing effect of nitrogen. It should be pointed out that the ferrite in austenitic stainless steel weld metal is a nonequilibrium phase and that any lack of good correlation between the composition and ferrite content could result from a number of other factors. For one, the ferrite morphology as influenced by the mode of solidification and subsequent solid state transformations may also contribute to the variations in measured ferrite content within the weld.

A relationship between ferrite content and weld metal microstructure has been observed.[12] However, the thermal cycles to which some of the initial weld passes are subjected during a multipass weld are another factor that could contribute to the observed variations within the weld metal. Since the ferrite in the weld metal is not an equilibrium structure, thermal cycling could dissolve it, thus bringing about a change in ferrite content of the weld from region to region. In addition, the ferrite could transform in part to a nonmagnetic sigma phase.

The effect of cooling rate on ferrite content has been demonstrated[4] by the excessive amount of ferrite produced in a commercial wrought Type 347 alloy that was cooled rapidly. This alloy would normally have had little or no ferrite. In addition, little or no ferrite has been produced in rapidly cooled electron beam welded Type 312 stainless steel. Slower cooling rates normally produce well over 20 vol-% ferrite in this alloy. Similar observations have been made by David and Vitek[19] during the high-power laser welding of Type 308 stainless steel at welding speeds exceeding 24 mm/s (57 ipm). It should be pointed out that these cooling rates represent extremes. Producing metastable structures under extremely rapid or slow cooling is not very unusual.[20]

Our purpose was to identify and classify different ferrite morphologies in austenitic stainless steel welds and offer possible explanations as to their origins. In addition, we identified various factors that influenced the ferrite content of the weld metal.

*$Cr_{eq} = Cr + Mo + 1.5\ Si + 0.5\ Nb$, and $Ni_{eq} = Ni + 30\ C + 0.5\ Mn + 30\ N$. The nitrogen content of the weld metal was analyzed to be 0.04.

Table 1—Welding parameters

Welding arc:	
Electrode	0.16 in. (4.1 mm) long, 2% ThO_2—W
Electrode top	30 deg included angle with 0.075 in. (1.9 mm) flat
Shielding gas	75 He—25 Ar (vol—%), 30 cfh (2.4 × 10^{-3} m^3/s)
Backup gas	Argon
Arc voltage	15 V
Current	350 A dcsp
Hot wire:	0.045 in. (1.1 mm) long
Voltage	7 V
Current	80 A

Experimental Procedure

Welding

Two multipass welds were deposited on 1 in. thick (25 mm) Type 304L stainless steel plate [0.019 C, 1.75 Mn, 0.029 P, 0.006 S, 0.63 Si, 18.55 Cr, 10.0 Ni, and balance Fe (wt-%)] containing a single-V butt joint. One of the two welds was made with joint surfaces buttered with the weld metal and the other without buttering. The welds were made with Type 308 stainless steel filler metal [0.016 C, 0.35 Si, 0.004 S, 0.029 P, 1.95 Mn, 9.76 Ni, 20.14 Cr, and balance Fe (wt-%)] by the hot-wire gas tungsten arc process (GTA). The welding parameters are given in Table 1.

Each weld consisted of eight passes. Samples for FN measurements were taken after each pass, and the average ferrite number of the root pass was measured after each pass. Ferrite number was measured by magnetic permeability with a Magne-gage instrument. The FN was measured in accordance with AWS A4.2-74, "Standard Procedures for Calibrating Magnetic Instruments to Measure the Delta Ferrite Content of Austenitic Stainless Steel Weld Metal."

Melting and Casting

To characterize structures resulting from extreme variations in solidification conditions, additional specimens were prepared by using several alternate techniques. Samples were cooled at estimated[21] rates ranging from 12 to 65°C/s (54 to 149°F/s) by drop casting arc melted Type 308 stainless steel filler metal (of composition described earlier) into a water-cooled copper mold described elsewhere.[22] In addition, two other cooling rates, one estimated[23] to be 1600°C/s (2912°F/s) and the other measured to be 7°C/s (45°F/s), were obtained by quenching 0.08 to 0.1 in. diameter (2-3 mm) filler metal droplets in iced water and casting a 2 in. diameter (50 mm) bar into a graphite mold, respectively.

Microstructural Characterization

Standard metallographic techniques for austenitic stainless steels were used for microstructural analysis. The samples were etched with a solution containing five parts concentrated HCl to one part concentrated HNO_3. The secondary dendrite arm spacings were measured by using a filar eyepiece. To investigate the ferrite morphology, small volume elements containing representative ferrite morphologies were cut out from the weld and polished on three orthogonal planes.

Foils of weld metal for electron microscopic analysis were electropolished with a dual jet polishing apparatus and a solution of 10 vol-% perchloric acid in methanol. The samples were polished at 17°F (—10°C) with 55 V dc. To determine if any precipitate particles were in the weld metal, electrolytic extractions were performed on the weld. The extracted precipitate particles were then analyzed by x-ray diffraction. The details of the extraction and x-ray procedures are reported elsewhere.[24]

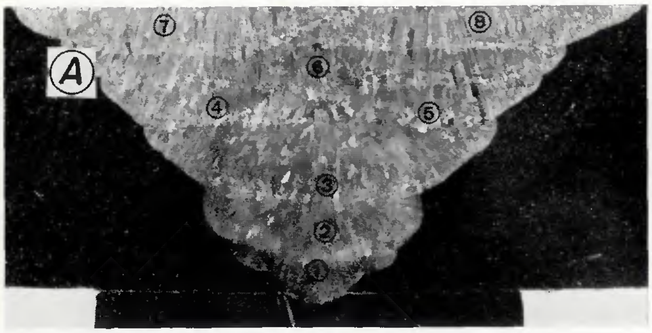

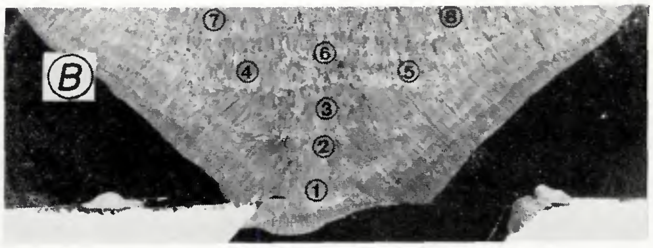

Fig. 1—Cross sections of Type 308 stainless steel multipass welds. Base plate is 1 in. (25 mm) thick: A—with unbuttered joint surfaces; B—with buttered joint surfaces

Weld Metal Microstructure and Ferrite Morphology

Macroscopic views of cross sections from the two welds are shown in Fig. 1. A wide variety of microstructures were observed at various locations within the multipass welds. The microstructure is duplex, with ferrite being the minor phase distributed in various forms in an austenite matrix.

To a great extent the solidification behavior and subsequent solid state transformations that occur within the weld metal on cooling control the microstructural characteristics of the weld metal. Suutala and co-workers[12] have described some of these microstructural features, relating them to different modes of solidification.

An earlier study[25] involving thermal analysis and interrupted solidification experiments revealed that the solidification sequences in Type 308 stainless steel filler metal include primary crystallization of δ-ferrite with subsequent envelopment by austenite. From the point of complete envelopment, further transformations $L \rightarrow \gamma$ and $\delta \rightarrow \gamma$ proceed at the δ-L and γ-δ interfaces. Further, as the sample cools to a temperature below that of the solidus, the transformation at the γ-L interface goes to completion, leaving behind a skeletal network of untransformed δ-ferrite along the cores of the primary and secondary dendrite arms. This residual ferrite has been shown to be enriched in chromium, which makes it very stable (Fig. 2). However, primary ferrite with a lower average chromium concentration of approximately 24 to 25 wt-% may transform to Widmanstätten austenite and ferrite during rapid cooling. During the above transformations extensive solute redistribution occurs by diffusion. These two modes of ferrite formation may be used to explain the various ferrite morphologies observed in austenitic stainless steel welds.

From the orthogonal sectioning of the volume elements extracted from various locations within the multipass weld with buttered joint surfaces, we have identified four distinct types of ferrite morphologies: type I—vermicular, type II—lacy, type III—acicular, and type IV—globular. Figure 3 shows three-dimensional views of these four ferrite forms. As stated earlier, austenitic stainless steel welds containing a duplex structure have no single representative microstructure.

All four morphologies shown in Fig. 3 were observed in the same multipass weld made with Type 308 stainless steel filler metal of constant Cr_{eq}/Ni_{eq} = 1.66. Also, the literature often characterizes ferrite morphology as continuous or discontinuous depending on the section of the weld viewed. We must be cautious in such characterization of the ferrite since only vermicular and lacy morphologies approach continuous shapes.

Type I—Vermicular Morphology

This type ferrite is the one most commonly observed in austenitic stainless steel welds containing duplex structure with FN 5 to 15. In the present investigation this particular morphology was predominantly observed in the weld root pass and the two subsequent passes. Depending on the sectional cut viewed, the ferrite could appear as an aligned skeletal network (FN 12) or as a curved soft form (FN 9), as shown in Fig. 3A. Further discussion of variation in ferrite number as a function of orientation follows. The alignment is along the heat flow direction, which is also the primary dendrite growth direction. The ferrite is located within the cores of the primary and secondary dendrite arms and is the result of the incomplete primary $\delta \rightarrow \gamma$ transformation discussed earlier. The classification of ferrite located at the intercellular or cellular dendritic

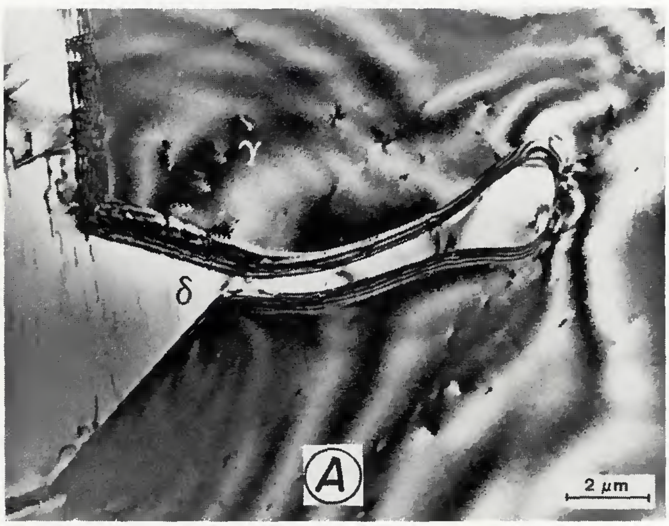

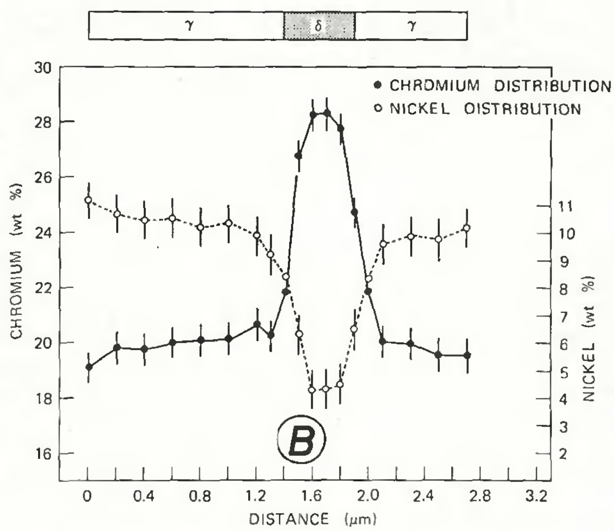

Fig. 2—Scanning transmission electron microscopy analysis of ferrite in the gas tungsten arc bead-on-plate weld: A—transmission electron micrograph; B—solute profiles across the ferrite

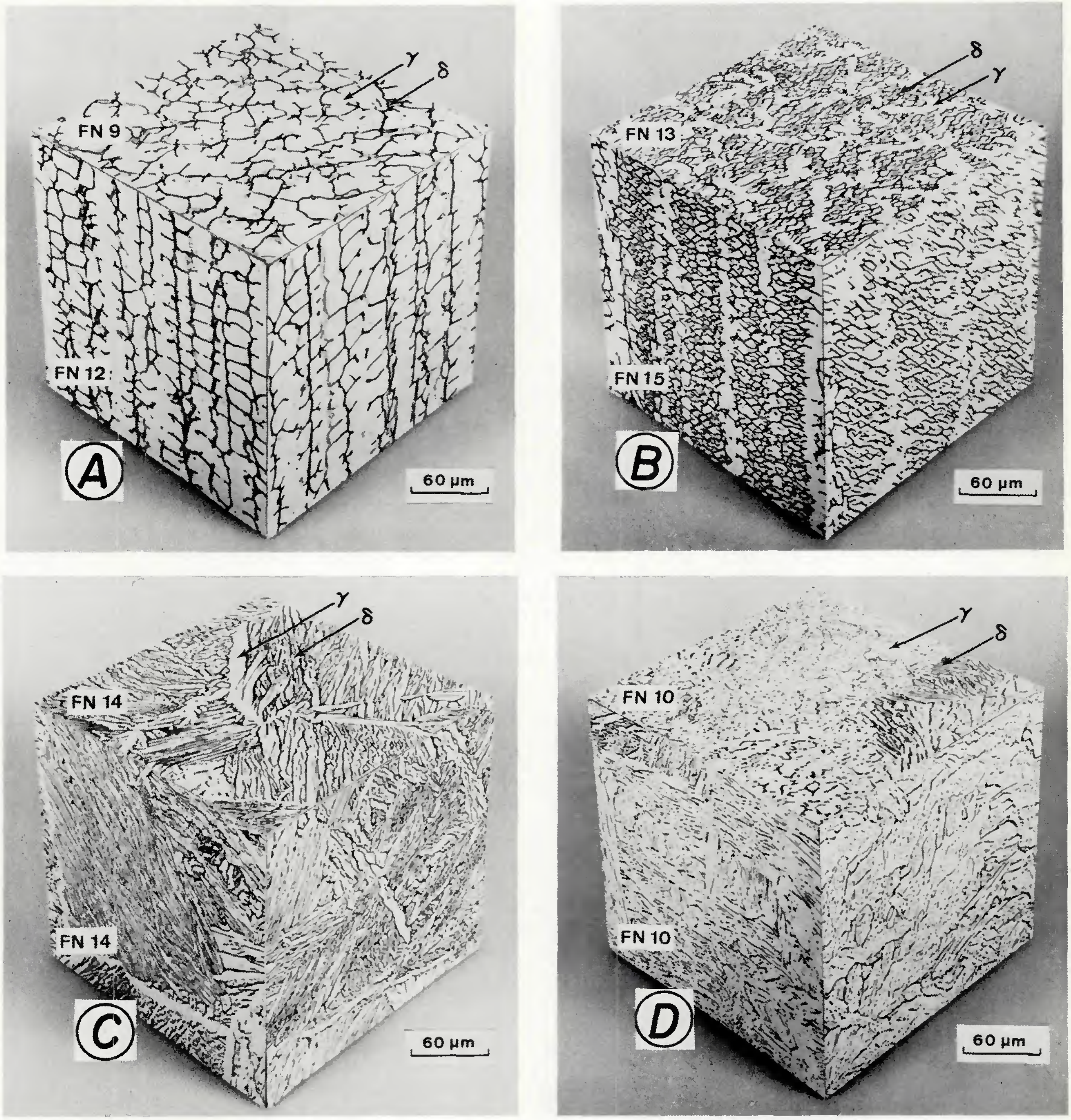

Fig. 3—Three-dimensional composite micrographs of various ferrite morphologies in Type 308 stainless steel multipass weld: A—type I, vermicular; B—type II, lacy; C—type III, acicular; and D—type IV, globular

boundaries in Type 310 stainless steel welds as vermicular by Suutala and co-workers[12] may be debatable since this ferrite would seldom tend to be continuous and vermicular. Often it is discontinuous and globular as shown later.

Type II—Lacy Morphology

The lacy form of ferrite is characterized by long columns of interlaced ferrite network oriented along the growth direction in an austenite matrix. This structure was predominantly present in the third pass of the weld. The structure looks very regular and aligned, as shown in Fig. 3B. The ferrite is located within the cellular dendrites.

Depending on the sectional cut viewed and the corresponding ferrite measurement, the duplex structure showed a FN 13 or 15. The origin of this ferrite morphology is likely to be the transformation of primary δ-ferrite cells to Widmanstätten austenite and ferrite, as discussed earlier.

Type III—Acicular Morphology

The acicular morphology is characterized by the random arrangement of needle-like ferrite distributed in an austenite matrix, as shown in Fig. 3C. This type structure was predominantly present in the sixth and crown passes of the weld (passes 7–8). Unlike the two morphologies described earlier,

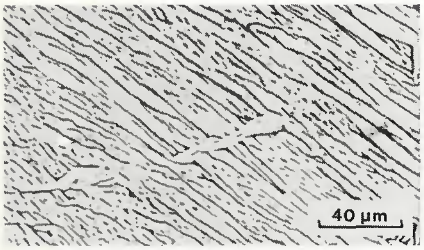

Fig. 4—The breakdown of acicular ferrite to globular ferrite in Type 308 stainless steel multipass weld

the structure here has no directionality and also does not seem to conform to the solidification substructure in any way. The average FN of the structure is 13. A similar structure has been observed in filler metal Types 318[12] and 312 stainless steel[26] with a high Cr_{eq}/Ni_{eq} ratio.

This ferrite morphology is typical of weld metals with $Cr_{eq}/Ni_{eq} > 2$. The presence of this particular ferrite form in the present weld ($Cr_{eq}/Ni_{eq} = 1.66$) could be attributed to local variations in composition, mainly macrosegregation. It should be pointed out that the last few passes were made by oscillating the weld head laterally from one side wall to the other to cover the width of the weld.

Such a motion, in addition to giving a complex puddle shape, would enhance turbulent fluid flow in the weld puddle, which could promote melting and/or breaking off of the chromium-rich cellular dendrites.[27] Such events, in turn, could bring about a change in liquid composition and the mode of solidification to $L \rightarrow L + \delta \rightarrow \delta$ and grain structure in localized regions. Further, the structure has its origin in the low-temperature transformation of primary ferrite that formed during solidification to austenite and ferrite. The austenite appears to have nucleated at the grain boundaries and grown inside the grains by an acicular mechanism.

Type IV—Globular Morphology

The globular form is characterized by ferrite in the form of globules randomly distributed in a matrix of austenite, as shown in Fig. 3D. As in the acicular form the structure has no directionality and is not related to the overall solidification substructure. It is commonly observed in weld passes 4, 5, and 6 of the multipass weld. Along with passes 1 through 3, these passes were also subjected to thermal cycling during welding. This structure typically has an average FN of 10. The structure appears to have its origin in the thermal instability of any of the other types of ferrite, particularly the acicular form.

The thermal cycles to which some of the weld passes are subjected in a multipass weld seem to bring about shape instabilities of a type described later. As a result of the shape instability, the long thin ferrite needles in the acicular structure and the interlaced ferrite in the lacy structure could break down into small disconnected globules. Figure 4 shows such a microstructural instability in the acicular morphology of ferrite. In addition to the thermal effects, stress during thermal cycling could intensify microstructural instability, which is very common in materials containing duplex structures, particularly aligned eutectics.[28]

The globular morphology of ferrite may also be seen in Type 310 stainless steel welds [0.11 C, 1.64 Mn, 0.014 P, 0.009 S, 26.73 Cr, 21.15 Ni, and balance Fe (wt-%)], where a very low volume fraction of ferrite in globular form may be present in the intercellular or interdendritic region, as shown in Fig. 5. The ferrite here is very discontinuous and forms as a result of the continuous enrichment of chromium in the liquids ($K^{\gamma L}_{Cr} < 1$)* during solidification.

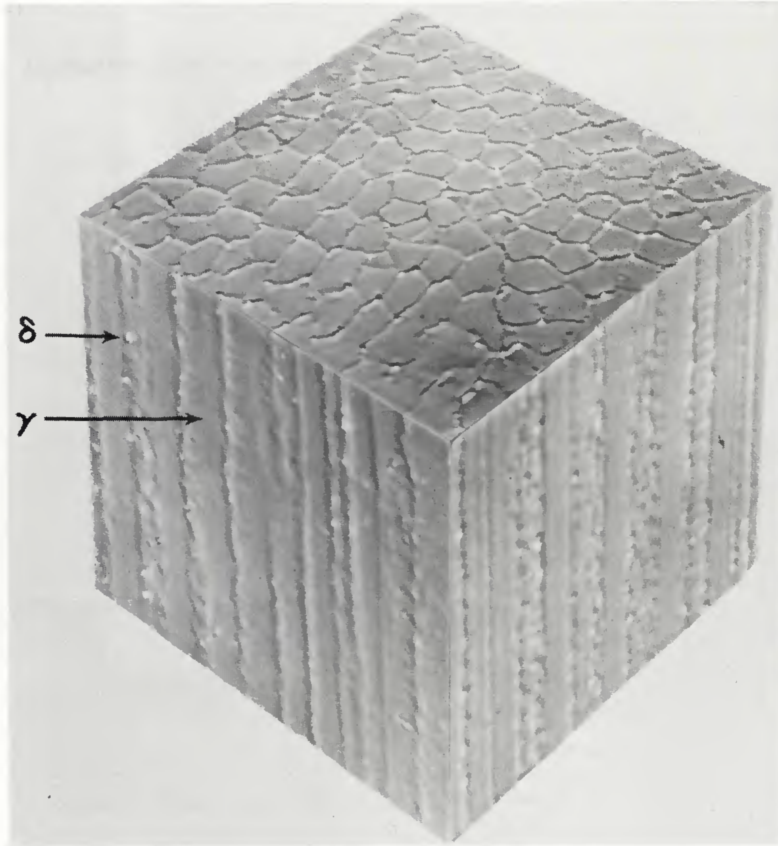

Fig. 5—Three-dimensional composite micrograph showing cellular structure in Type 310 stainless steel weld metal with ferrite in globular form located in the intercellular regions

**Equilibrium partition ratio $K^{\gamma L}_{Cr} = C^{\gamma}_{Cr}/C^{L}_{Cr}$ where C^{γ}_{Cr} and C^{L}_{Cr} are the chromium concentrations in austenite and liquid given by the tie line at a particular temperature.*

Variations in Ferrite Content

As stated earlier, a number of factors such as composition, ferrite morphology, ferrite dissolution and/or transformation, and cooling rate may influence the amount of ferrite present within the weld deposit. Any such variation in ferrite content from location to location within the weld may influence its mechanical and chemical behavior.

Figure 6 shows the variation in the root pass FN within the two welds in our study. In weld 1 (top curve) the base-metal joint surfaces were buttered with the weld metal, while in weld 2 (bottom curve) the base metal joint surfaces were not buttered. The average FNs of the root pass deposit in welds 1 and 2 are 13 and 8, respectively. The lower FN of the root pass deposit in weld 2 is attributable to the weld metal dilution with the base metal and hence indicates a change in the weld metal composition.

In practice, the extent of dilution depends on the welding process and procedure variables such as current, travel speed, welding technique, joint design, and material thickness. The further decrease in FN of the root pass deposit in both welds results from the

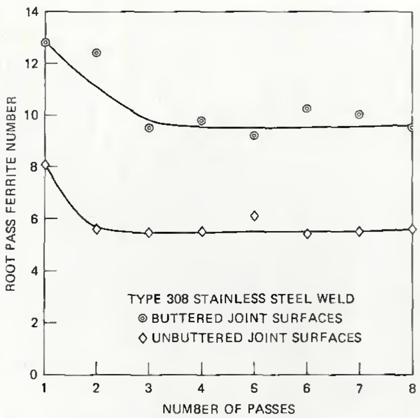

Fig. 6—Variations in root pass ferrite number with subsequent passes in welds made with buttered and unbuttered joint surfaces

Fig. 7—Transmission electron micrograph showing the absence of transformation products in a sample taken from the root pass of the Type 308 stainless steel multipass weld

dissolution of ferrite from the thermal effects to which the root pass is subjected during a multipass weld. The dissolution of ferrite is discussed in great detail later in this paper.

In addition to the observed thermal effects during subsequent passes on the FN of the root pass, variations in FN were observed in both welds within a cross section of the bead, along the length and width of the weld, and from bead to bead. Generally, the FN increased from the root pass to the crown pass. The ferrite content within the weld at various locations varied from 5 to 14 and 9 to 13 for the welds with unbuttered and buttered joint surfaces, respectively.

Some of these variations are attributable to dilution effects (particularly in the weld made with unbuttered joint surfaces); thermal effects; and other factors such as ferrite morphology, dissolution of ferrite, and cooling rate to be discussed shortly. Here, we should also mention possible changes in the amount of nitrogen pickup during welding, which could contribute in part to variations in ferrite content.

The FN associated with various ferrite morphologies is closely related to the volume percent of ferrite and in turn the composition. As discussed earlier, the orientation of the ferrite with respect to surface examined could bring about a minor variation in FN. The FN associated with each morphology is shown in Fig. 3. For example, the FN for type I vermicular morphology varied from 9 to 12, depending on which section the magnetic measurements were made. Although quantitative metallography showed no drastic variations in the volume percent of ferrite for the top and side views, the magnetic measurements showed a definite difference in FN. The same observation was true for type II lacy morphology. Hence, the difference in FN seems to be related to the microstructural continuity and the interaction of the magnetic flux with the ferrite.

Dissolution of the ferrite from subsequent thermal cycles in a multipass weld is another factor that could contribute to the variations in ferrite content. Figure 6 shows such a variation in root pass FN for the welds 1 and 2 as a function of seven other subsequent passes. Results show a drastic reduction in root pass FN for both welds with the first three subsequent passes, after which the FN remains constant. An extensive microstructural analysis of the root pass in welds 1 and 2 indicated that the reduction in ferrite results from its dissolution during the thermal excursions of the weld. Chemical extraction from samples of the welds revealed no precipitates.

Figure 7 is a transmission electron micrograph of a sample taken from the root pass deposit of weld 1 showing ferrite in an austenite matrix. No precipitation of any kind was observed at the γ-δ interface or within the delta phase. The observed absence of transformation products is typical of the investigated Type 308 stainless steel weld metal only. Transformation of ferrite to sigma from thermal cycle effects in a multipass weld is possible for weld metals of different compositions.

An investigation of the effect of solidification rate on the ferrite content has led to some interesting conclusions. It has been suggested that the increase or decrease in ferrite content of austenitic stainless steel weld metal caused by a decrease or increase in solidification rate, respectively, provides an alternate method other than composition for varying the ferrite content.[29] This variation in ferrite level as a function of solidification rate is closely related to the kinetics of primary $\delta \rightarrow \gamma$ transformation.

It is a well established fact that the solidification substructure size (primary or particularly secondary dendrite arm spacing) is a strong function of local solidification time θ_f defined for a point in the weld as the difference in time between the passing of the liquidus and solidus isotherms.[30] Therefore,

$$d = C\theta_f^n \ (0.3 < n < 0.5), \qquad (1)$$

where d is the dendrite arm spacing and C is a constant. Thus, the dendrite arm spacing would be finer for high solidification rates and coarser for low solidification rates.

The kinetics of primary $\delta \rightarrow \gamma$ transformation depend greatly on the diffusion distances as determined by the dendrite arm spacing. Therefore, avoiding any extreme nonequilibrium situations, the higher the solidification rate (within the realm of normal welding processes), the finer the spacing of the substructure. Hence, a greater amount of primary ferrite would transform to austenite in a given time, resulting in lower ferrite content in the microstructure. The amount of ferrite would be optimum as determined by the effects from the two opposing factors—short time at high temperature and finer spacing of the dendrite substructure.

Postsolidification heat effects also contribute to the $\delta \rightarrow \gamma$ transformation. Similarly, for low solidification rates, the solidification substructure would be coarser and hence a large amount of primary ferrite would remain untransformed to austenite. The extent of solute redistribution involved could also contribute to the extent of this reaction via chromium partitioning and buildup within the ferrite, thus contributing to its stability. In addition, all the above could be altered by superposition of postsolidification heat effects.

During the present investigation ferrite measurements on samples solidified at various cooling rates showed very little variation in the ferrite content (Fig. 8). An average FN for each sample was obtained by measuring the FNs on different sections of the sample to avoid effects of orientation. Also, a water-quenched Type 308 filler metal droplet had an FN of 6.1 and that of the slowly cooled small ingot sample of the same alloy had an FN of 7.0, as shown in Fig. 8 by the closed circle and triangle, respectively. However, it should be pointed out that in the slowly cooled sample, postsolidification heat effect may have contributed to a certain amount of reduction in the ferrite content.

The role of solidification rate and the associated substructural size on the ferrite dissolution kinetics and hence the ferrite content can be elucidated as follows. Figure 8 shows the change in ferrite content at 1832°F (1000°C) for different times on three samples of Type 308 stainless steel filler metal used in this investigation with three different secondary dendrite arm spacings. The rate of change of FN is higher for the sample with finer dendrite arm spacing than for the one containing coarse dendrite spacings. As discussed earlier this is attributable mostly to the dissolution rate of ferrite being higher in samples containing finer dendrite spacing than in the one having coarser spacing.

The structure of a cast Type 308 stainless steel sample [secondary dendrite arm spacing of 1.00 mil (25.5 μm)] before and after the 1832°F (1000°C) heat treatment for 900 s is shown in Fig. 9. The arrows indicate evidence of ferrite dissolution. In addition, electrolyte extraction of specimens from these samples revealed $M_{23}C_6$, although the presence of a small amount of sigma could not be ruled out because of its possible dissolution during the extraction procedure.

Shape Instability of Ferrite in the Weld

To determine the microstructural stability of various ferrite morphologies, four samples containing the morphologies identified earlier were heat-treated for 10 min at 1922°F (1050°C). All the samples showed extensive degradation in the micromorphology of the ferrite. Figure 10 compared with Fig. 3 shows the extent of change in morphology observed in various samples.

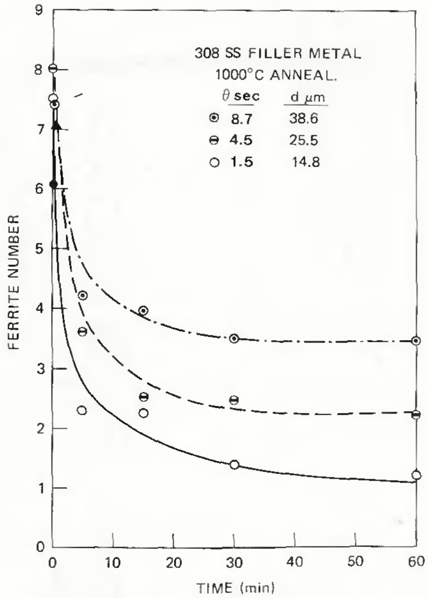

Fig. 8—Effect of heat treatment on the ferrite number in Type 308 stainless steel filler metal castings solidified at various cooling rates

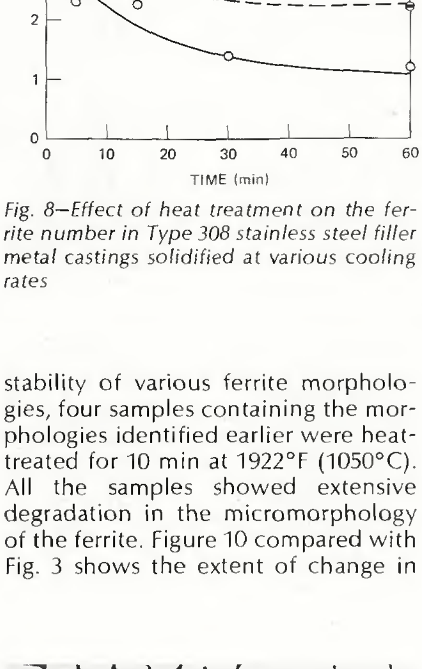

Fig. 9—Type 308 stainless steel filler metal casting [secondary dendrite arm spacing of 1.00 mil (25.5 μm)]: A—untransformed ferrite network before heat treatment; B—dissolution of ferrite upon heat treatment at 1832°F (1000°C) for 900 s

Figure 10A shows the breakdown in morphology of type I ferrite. On exposure to high temperature for short times, the ferrite seems to assume a rugged cylindrical form (with reduced δ-γ interfacial area) and further breaks down into rows of spherical particles. The phenomenon appears very similar to the Rayleigh instability,[31] which describes the breakdown of a liquid cylinder into a row of spherical droplets. It should be pointed out that the ferrite in the weld metal is a nonequilibrium phase and could dissolve at temperatures above the γ-($\sigma + \gamma + \delta$) phase boundary but below the γ-($\gamma + \delta$) solvus. Also, the observed ferrite shape in type I of sharp edges and curved surfaces (γ-δ interface) with sufficiently large ratio of surface area to volume is not the most stable ferrite morphology.

Ferrite of such shape will generally have differences or gradients in chemical potential of the constituent atoms as a result of capillarity.* Therefore, on exposure to high temperatures, two equilibrating processes proceed simultaneously: one being changes in ferrite shape leading to the formation of spherical particles with reduced interfacial area and associated interfacial energy and the other being dissolution of δ-ferrite. The former process results from the diffusive transport under the driving force of capillarity.[32] The sequence of events that occurs is shown schematically in Fig. 11. The simultaneous dissolution of δ-ferrite adds another dimension to the complexity of treating shape effects quantitatively. Shape instability such as the one described above has been observed in other materials containing duplex structures, particularly eutectics, with one major difference being that the volume fraction of the second phase in the eutectic remains almost constant. The phenomenon has been treated quantitatively by Cline.[28]

The morphological instability of type II ferrite on exposure to high temperature is shown in Fig. 10B. Here the well interlaced ferrite gets disconnected randomly during the dissolution process and sometimes assumes a globular morphology. Given sufficient time this could lead to complete dissolution of ferrite in austenite.

Type III ferrite on exposure to high temperature breaks down into rows of well spaced spherical particles, as shown in Fig. 10C. The problem here again appears to be one of shape instability accompanied by dissolution of ferrite. Finally, on exposing the sam-

The effect of curvature of a surface on the chemical potential of the surface atoms.

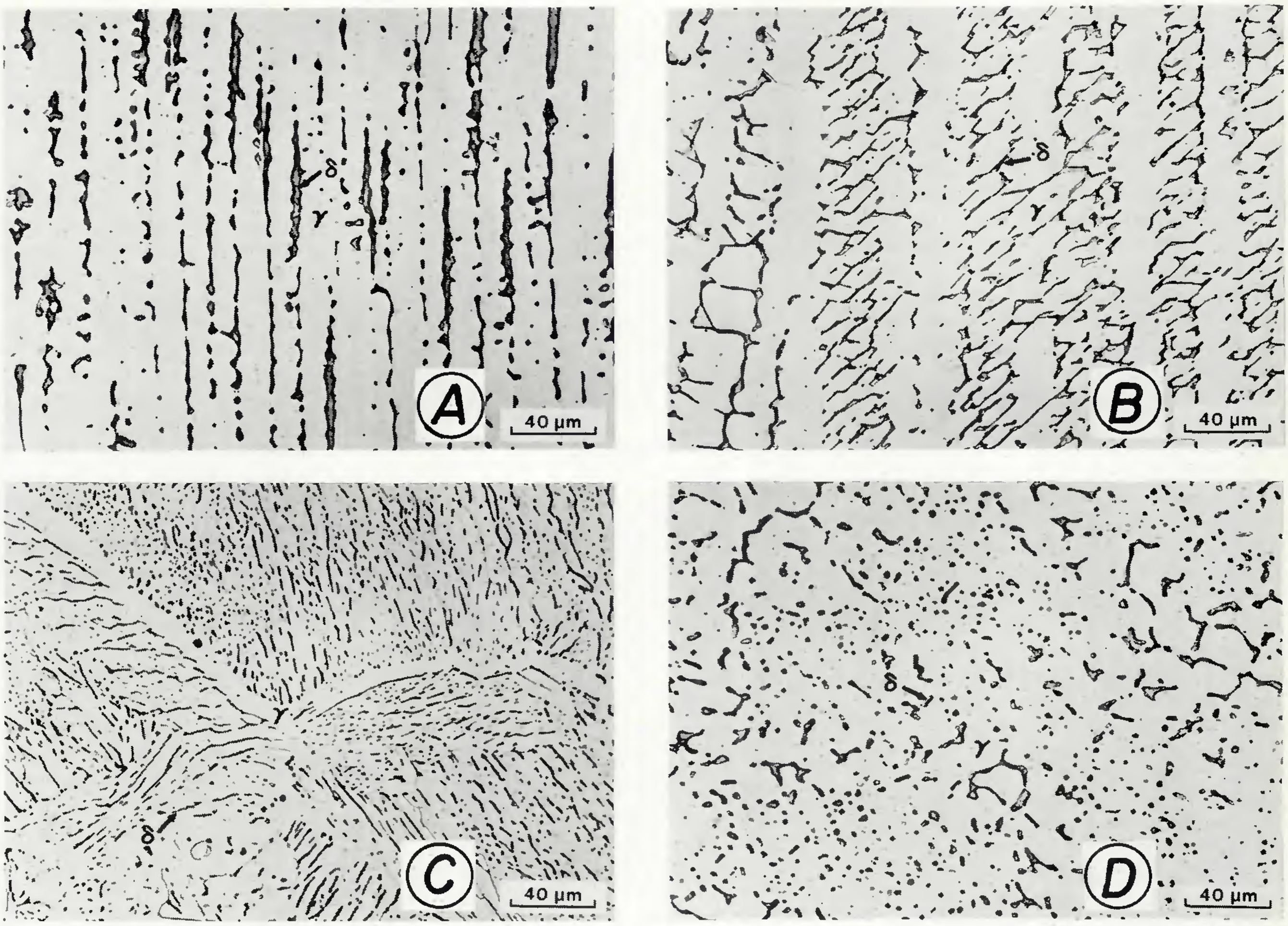

Fig. 10—Shape instabilities in various ferrite morphologies: A—type I, vermicular; B—type II, lacy; C—type III, acicular; D—type IV, globular

ple containing type IV ferrite (globular), the microstructure changed little except more of the ferrite globules went into solution.

Conclusion

Four distinct types of ferrite morphologies have been identified in Type 308 stainless steel multipass welds with FN's ranging from 9 to 15: vermicular, lacy, acicular, and globular. The first three types are related to solidification and transformations following solidification. The fourth type is related to the shape instability of any of the other three types of ferrite because of thermal effects.

The origin of the three types of ferrite may be explained by the various modes of ferrite formation in austenitic stainless steel welds containing a duplex structure. They are residual primary ferrite resulting from incomplete $\delta \rightarrow \gamma$ transformation during solidification and/or residual ferrite after Widmanstätten austenite precipitation. The origin of the fourth type of ferrite may be explained on the basis of ferrite shape instability at elevated temperatures leading to the formation of spherical particles under the driving force of capillarity. At the same time there is dissolution of δ-ferrite in austenite.

Ferrite content within the weld at various locations varied from 5 to 14 and 9 to 13 for the welds with unbuttered and buttered joint surfaces, respectively. The variations are closely related to the weld composition, ferrite morphology, and dissolution of ferrite during thermal cycles experienced by the weld metal from subsequent weld passes. Weld metal solidification rates encountered within the confines of common welding processes may not significantly affect the ferrite content. However, the scale of the solidification substructure associated with various solidification rates may influence the ferrite dissolution or transformation kinetics.

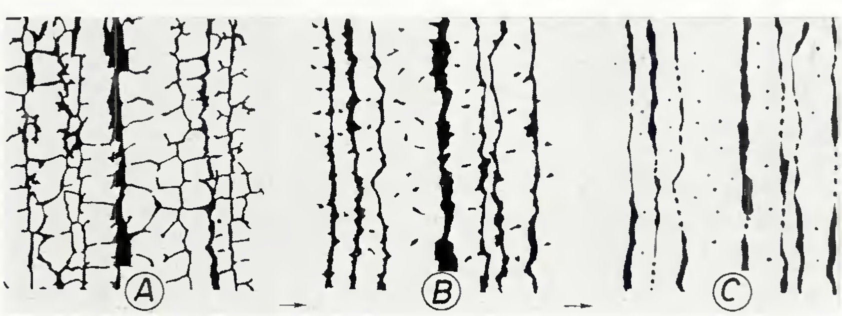

Fig. 11—Sequence of events in the shape instability of ferrite

Acknowledgments

The author gratefully acknowledges C. J. McHargue, Program Manager, for encouragement and support; V. T. Houchin and C. P. Haltom for welding and metallography, respectively; and S. E. Hanzelka for magnetic measurements. He also acknowledges J. W. McEnerney and G. M. Goodwin for technical discussions, J. O. Steigler and C. T. Liu for reviewing the manuscript, B. G. Ashdown for editing, and S. G.

Frykman for preparing the manuscript for publication.

The research discussed in this paper was sponsored by the Division of Materials Sciences, U. S. Department of Energy, under contract W-7405-eng-26 with the Union Carbide Corporation.

References

1. Borland, J. C., and Younger, R. N., "Some Aspects of Cracking in Austenitic Steels," *British Welding Journal*, 7(1), Jan. 1960, pp. 22-60.

2. Hull, F. C., "Effect of Delta Ferrite on the Hot Cracking of Stainless Steel," *Welding Journal*, 46(9), Sept. 1967, Research Suppl., pp. 399-s to 409-s.

3. Arata, Y., Matsuda, F., and Katayama, S., "Solidification Crack Susceptibility in Weld Metals of Fully Austenitic Stainless Steel (Report I)—Fundamental Investigation on Solidification Behavior of Fully Austenitic and Duplex Microstructures and Effect of Ferrite on Microsegregation," *Transactions of the Japanese Welding Research Institute*, 5(2), Feb. 1976, pp. 35-51.

4. DeLong, W. T., "Ferrite in Austenitic Stainless Steel Weld Metal," *Welding Journal*, 53(7), July 1974, Research Suppl., pp. 273-s to 286-s.

5. Hauser, D., and VanEcho, J. A., *Properties of Steel Weldments for Elevated Temperature Pressure Containment Applications*, MPC-9, Smith, G. V., ed., American Society of Mechanical Engineers, New York, 1978, pp. 17-46.

6. Edmonds, D. P., Vandergriff, D. M., and Gray, R. J., *Properties of Steel Weldments for Elevated Temperature Pressure Containment Applications*, MPC-9, Smith, G. V., ed., American Society of Mechanical Engineers, New York, 1978, pp. 47-61.

7. Castro, R., and de Cadenet, J. J., *Welding Metallurgy of Stainless and Heat Resisting Steels*, Cambridge University Press, London, 1974.

8. Viswanathan, R., Nurminen, J. I., and Aspden, R. G., "Stress Corrosion Behavior of Stainless Steel Welds in High Temperature Water Containing Chloride," *Welding Journal*, 58(4), Apr. 1979, Research Suppl., pp. 118-s to 126-s.

9. Devine, T. M., "Influence of Ferrite Morphology and Carbon Content on the Sensitization of Duplex Stainless Steel," Abstract, 109th AIME Annu. Meeting, Las Vegas, Nevada, February 1980.

10. Estes, C. L., and Turner, P. W., "Dilution in Multipass Welding AISI 4130 to Type 304 Stainless Steel," *Welding Journal*, 43(12), Dec. 1964, Research Suppl., pp. 541-s to 550-s.

11. Goodwin, G. M., Cole, N. C., and Slaughter, G. M., "A Study of Ferrite Morphology in Austenitic Stainless Steel Weld Metals," *Welding Journal*, 51(9), Sept. 1972, Research Suppl., pp. 425-s to 429-s.

12. Suutala, N., Takalo, T., and Moisio, T., "Relationship Between Solidification and Microstructure in Austenitic and Austenitic-Ferritic Stainless Steel Welds," *Metallurgical Transactions*, 10 A, 1979, pp. 512-14.

13. Takalo, T., and Moisio, T., "Single Phase Ferritic Solidification Mode in Austenitic-Ferritic Stainless Steel Welds," *Metallurgical Transactions*, 10 A, 1979, pp. 1183-90.

14. Lai, J. K., Nath, B., and Townsend, R. D., "Variations in Delta-Ferrite Content and Morphology in a Multipass Type 316 Weldment and Their Effect on Creep Rupture Properties," British Nuclear Energy Society, Conference on Welding and Fabrication in the Nuclear Industry, London, April 1979.

15. Takalo, T., and Moisio, T., "Influence of Ferrite Content on its Morphology in Some Austenitic Weld Metals," *Metallurgical Transactions*, 7 A, 1976, pp. 1591-92.

16. Schaeffler, S. L., "Constitution Diagram for Stainless Steel Weld Metal," *Metals Progress*, 56, Nov. 1949, pp. 680 and 680 B.

17. DeLong, W. T., Ostrom, G., and Szumachowski, E., "Measurement and Calculation of Ferrite in Stainless Steel Weld Metal," *Welding Journal*, 35(11), Nov. 1956, Research Suppl., pp. 526-s to 533-s.

18. Long, C. J. and DeLong, W. T., "The Ferrite Content of Austenitic Stainless Steel Weld Metal," *Welding Journal*, 52(7), July 1973, Research Suppl., pp. 281-s to 297-s.

19. David, S. A., and Vitek, J. M., Oak Ridge National Laboratory, Oak Ridge, Tenn., unpublished results.

20. David, S. A., and Brody, H. D., "Controlled Solidification of Peritectic Alloys," *Proc. Int. Conf. Solidification*, Metals Society, London, 1979, pp. 144-51.

21. Brody, H. D., University of Pittsburgh, Pa., to David, S. A., Oak Ridge National Laboratory, Oak Ridge, Tenn., private communication, June 1980.

22. Nurminen, J. I., and Brody, H. D., "Dendrite Morphology and Microsegregation in Titanium Base Alloys," *Titanium Science and Technology*, Vol. 3, Jaffee, R. I., and Burte, H. M., eds., Plenum Press, New York, 1973, pp. 1893-1914.

23. Kou, S., Carnegie Mellon University, Pittsburgh, to David, S. A., Oak Ridge National Laboratory, Oak Ridge, Tenn., private communication, October 1980.

24. Leitnaker, J. M., *et al.*, *Transformations Occurring on Aging of 16-8-2 Weld Metal*, ORNL-5400, Oak Ridge National Laboratory, June 1978.

25. David, S. A., Goodwin, G. M., and Braski, D. N., "Solidification Behavior of Austenitic Stainless Steel Filler Metals," *Welding Journal*, 59(11), Nov. 1979, Research Suppl., pp. 330-s to 336-s.

26. Lippold, J. C., and Savage, W. F., "Solidification of Austenitic Stainless Steel Weldments: Part I—A Proposed Mechanism" *Welding Journal*, 59(12), Dec. 1979, Research Suppl., pp. 362-s to 374-s.

27. Flemings, M. C., *Solidification Processing*, McGraw-Hill, New York, 1974, p. 229.

28. Cline, H. E., "Shape Instabilities of Eutectic Composites at Elevated Temperatures," *Acta Metallurgica*, 19, 1971, pp. 481-90.

29. Lundin, C. D., University of Tennessee, Knoxville, to David, S. A., Oak Ridge National Laboratory, Oak Ridge, Tenn., personal communication, December 1977.

30. Brody, H. E., and David, S. A., "Application of Solidification Theory to Titanium Alloys," *Proc. Science Technology and Application of Titanium*, Jaffee, R., and Promisel, N., eds., Pergamon Press, New York, 1970, pp. 21-34.

31. Lord Rayleigh, *London Mathematical Society Proc.*, 10, 1879, p. 4.

32. Mullins, W. W., "Metal Surfaces," *ASM Transactions Quarterly*, 1963, pp. 17-66.